Food Engineering Reviews (2021) 13:225–235
https://doi.org/10.1007/s12393-020-09247-8

The Influence of Operation Parameters and Product Properties on Time-to-Temper for Frozen Raw Meat Based on Simulation

Shengyue Shan[1] · **Dennis R. Heldman**[1]

Received: 22 January 2020 / Accepted: 31 July 2020 / Published online: 27 August 2020

Abstract
Tempering is a unit operation of increasing the temperature of the frozen food to an optimal temperature for further processing, usually below its freezing point. In the meat industry, tempering occurs prior to slicing, dicing, cutting, or other steps. This study recommended a definition of time-to-temper based on temperature distribution uniformity. A transient heat transfer model was established with MATLAB PDE toolbox in finite element method (FEM) to generate temperature distribution histories within the studied pork products, which provides faster computation and more straightforward data postprocessing. The temperature-dependent thermophysical properties of the frozen products have been predicted based on product composition. The simulated results provide an illustration of the temperature distribution history during tempering. The effects of convective heat transfer coefficient (h), ambient temperature (T_a), product composition, and product dimension on time-to-temper have been compared and discussed. Increasing h-value reduces time-to-temper effectively only in the range of 0 to 200 $W{\cdot}m^{-2}{\cdot}K^{-1}$; further increase in h does not significantly decrease time-to-temper. T_a below freezing point of the product leads to relatively short time-to-temper, and the highest time-to-temper usually occurs when T_a is around 1 °C higher than the product freezing point. When product thickness increases, time-to-temper increases at a higher ratio than that of thickness increase.

Keywords Time-to-temper · Frozen meat · Heat transfer simulation

Introduction

Meat is known as a highly shelf-unstable food [6] such that it is usually kept frozen during the transportation for quality preservation [28]. Microbial activities, which are the major factor for the deterioration in meat, are effectively inhibited [28] under the low-temperature condition of frozen storage (typically −20 to −18 °C, which may be as low as −80 °C for high-value fish [14]). However, adverse effects of freezing, such as protein denaturation and myofibrillar aggregation, damage the water-holding capacity of meat muscle, increase the fluid exudation (drip loss), and increase toughness in the thawed meat [28].

In industry, frozen meat usually needs to be thawed or tempered before further processing, such as cutting, dicing, and slicing [6]. Thawing is increasing the temperature of the product until the temperature of the coldest location is above the freezing point of the product [11], and comparatively, a lower target temperature of the product should be reached after tempering. The optimal target temperature of tempering is often determined by the next processing step requirement, but ideally, the hottest location in the product should be kept under its freezing point [11], within the range of −5 to −2 °C [14]. Compared with thawing, tempering is a more preferred temperature increasing operation due to the lower processing temperature, and consequently, there is reduced risk of microbial or chemical deterioration drip loss [13]. The physical properties of meat related to further processing, such as hardness, are determined by the temperature and ice content of the the product. It is preferred to maintain a small temperature gradient within the product, as it is usually difficult for the downstream facilities, e.g., cutter, slicer, or grinder, to operate over a variety of hardness [3]. Aside from uniformity of temperature, it is also required that the target temperature of tempering should not be too high nor too low. If overly tempered, the product may be too soft and thus will tear and deform in further processing. If undertempered, the product may be too hard, resulting in

✉ Shengyue Shan
shan.131@osu.edu

[1] The Ohio State University, 2015 Fyffe Road, Columbus, Ohio, 43210, USA

the need for more energy in subsequent unit operations or even damage to machinery [3].

Different methods of operations have been applied to tempering meat product, and innovative methods such as microwave (MW)-assisted tempering and radiofrequency (RF) are gaining more attention. However, limited penetration depth [6] and thermal runaway phenomena [23] of MW may lead to non-uniform heating and local overheating. RF is of greater potential for industrial application because it has greater penetration depth and results in more uniform heating, but the health risks brought by RF and the current lack of data related to RF application restrict the industrial application of RF [21]. Furthermore, installation and operation costs of innovative tempering systems are high, which also limits the application of innovative tempering methods in the industry. Therefore, the conventional method remains the most widely used tempering method for its easy implementation and controllable process, which is usually placing the product in water or air at a desired temperature.

The conventional tempering method utilizes convective heat transfer, where the efficiency is externally affected by the ambient temperature (T_a) and the convective heat transfer coefficient (h) [10]. In this study, T_a refers to the temperature of the tempering fluid. The h-value is directly related to the fluid velocity: increasing fluid velocity results in an increase in h-value. At a given velocity, the h-value for water is usually higher than that for air. It is generally considered that increasing T_a and h can reduce tempering time. However, high T_a may lead to significant temperature gradient within the product, leaving the product under the risk of surface spoilage. A high h-value will lead to higher energy cost for increasing the velocity of the tempering fluid. In addition, internal factors such as the composition and the dimensions of the product will also affect tempering time. The thermophysical properties, including thermal conductivity, density, and specific heat affected by the composition, will influence the heat transfer rate. Also, it tends to take a longer time to temper product with larger size. Therefore, it is important to understand the relationship between tempering time and these factors to improve tempering efficiency. The effects of external and internal factors on tempering time are both addressed in this study.

The heat transfer phenomenon occurring during tempering process can be described by a governing equation, which is usually a set of partial differential equations, along with initial and boundary conditions defined over a certain geometry [9]. For the tempering process of frozen food, difficulties are introduced to mathematical modeling by the phase change of water component in the product. Thermophysical properties tend to change sharply when approaching the product's freezing point, leading to a non-linearity in the governing equation [19]. Analytical solutions are attainable for simple phase change problems where only one substance is involved and phase change happens at a specific temperature point. However, for complex systems like food, in which phase change happens gradually over a range of temperature, numerical methods must be applied to deal with the complexity of the governing equation to obtain an accurate solution. The numerical methods that have been developed and commonly used include finite difference method (FDM), finite volume method (FEM), and finite element method (FEM). FDM is relatively easy to understand and implement. However, FDM is usually only applicable for geometries that can be discretized by orthogonal grids [19], and sometimes fails to satisfy the conservation laws when discretizing the governing equation [16]. FVM and FEM have rapidly developed over the past decades to accommodate multi-dimensional problems and irregular geometries. FEM has been successfully applied to solving 2D- or 3D-heat transfer problems in food processing, such as the air-blast cooling of roasted meat [27], anisotropic food freezing [12], and conduction and convection in refrigerated transportation [7]. The solutions for 2-D problems have been well researched, providing a solid basis for practical application. The geometry of the product studied in this investigation was not completely complex and irregular; therefore, with the assumptions introduced in section "MATLAB Partial Differential Equation Toolbox", this heat transfer process can be simplified to 2-D. The temperature distribution within this 2-D domain is of importance to determine whether the product has met the requirement for the next processing step. The 2-D simulation also has the advantages of faster computation and more straightforward interpretation of the results.

This study focuses on exploring the effects of external factors, T_a and h, and internal factors, product composition and dimension, on tempering time, which is defined as time-to-temper in the study. Time-to-temper is defined as the time when the location of the lowest temperature within the product reaches a target temperature and at the same time the temperature difference between this location and surface is relatively small. In previous research, time-to-temper is usually defined as the time when the average temperature [8] or the minimum temperature [17, 22] reaches a target temperature. However, these definitions fail to comprehensively describe the uniformity of temperature distribution, resulting in greater risk of temperature gradients which can be deleterious for subsequent unit operations. Additionally, meat products of different composition have different freezing points, and the relationship between temperature and physical properties of products may vary too. It is difficult to suggest a common target temperature that is applicable for different products, but the uniform temperature distribution is a common requirement despite the product composition. Therefore,

the time-to-temper defined in this study is suggested for practical use. The temperature distribution during the tempering process within the product was solved with MATLAB PDE toolbox. Pork loin, pork belly, and pork fat were selected as model systems in this investigation. The effects of T_a, h, product dimension on time-to-temper were demonstrated with pork loin. Pork belly and pork fat, which are of different water, protein, and fat content, were compared with pork loin to reveal the effects of product composition on time-to-temper.

The objectives of this study are (1) to simulate the temperature distribution within a frozen product during tempering; (2) to provide a mathematical definition of time-to-temper based on temperature distribution; (3) to illustrate the effects of ambient temperature, convective heat transfer coefficient, product composition, product geometry on time-to-temper.

MATLAB Partial Differential Equation Toolbox

The height, width, and length for the analyzed geometry is 6 cm, 30 cm, and 70 cm, respectively. The following assumptions were made for the demonstrated tempering process: (1) The product is a homogenous mixture of all components. (2) Ambient temperature (T_a), which represents the temperature of the tempering fluid in this case, is constant during tempering. (3) The post-processing step is slicing, which happens perpendicularly to the length direction. (4) Products are placed vertically in the tempering fluid, indicating that the heat conduction through the width-height cross section (area 6 cm× 30 cm as shown in blue in Fig. 1) is significant. (5) The convection happens at all four edges of the cross-section. (6) There is no heat generation within the product. (7) There is no drip loss of the product during tempering.

The industrial tempering operation is usually immersing the product in water or air of a certain temperature, which is a convective heat transfer process. For the studied case, the heat transfer in the height and width direction is more dominating, and the slicing happens on the height-width plane; therefore, the temperature distribution on this plan is of higher interest to guarantee the temperature uniformity necessary for defining the optimal state for the next processing step. Thus, the process could be simplified as a 2-dimensional transient heat transfer problem for faster computation and more straightforward data post-processing.

The governing equation for the heat transfer process was described in Eq. 1, with the initial condition Eq. 2 over the domain and boundary conditions Eq. 3a to Eq. 3d on all the four edges of the geometry.

$$\frac{\partial T}{\partial t} = \frac{\partial}{\partial x}\left(\alpha(T)\frac{\partial T}{\partial x}\right) + \frac{\partial}{\partial y}\left(\alpha(T)\frac{\partial T}{\partial y}\right)$$

$$\alpha(T) = \frac{k(T)}{\rho(T)c_p(T)} \tag{1}$$

$$T(x, y, 0) = T_0 \tag{2}$$

$$\text{At x = 0: } -k\frac{\partial T(0,y,t)}{\partial x} = h(T - T_a) \tag{3a}$$

$$\text{At x = L: } -k\frac{\partial T(L,y,t)}{\partial x} = h(T - T_a) \tag{3b}$$

$$\text{At y = 0: } -k\frac{\partial T(x,0,t)}{\partial y} = h(T - T_a) \tag{3c}$$

$$\text{At y = H: } -k\frac{\partial T(x,H,t)}{\partial x} = h(T - T_a) \tag{3d}$$

Where T is temperature (unit, °C), t is time (unit, s), x, y are the location coordinates (unit, m). α, k, ρ, and c_p are thermophysical properties, and are thermal diffusivity (unit, $J{\cdot}kg^{-1}$), thermal conductivity (unit, $W{\cdot}m^{-1}{\cdot}K^{-1}$), density (unit, $kg{\cdot}m^{-3}$), and specific heat (unit, $J{\cdot}K^{-1}$). T_0 is the initial temperature for the product (unit, °C). x_s, y_s are the surface location coordinates (unit, m), h is the convective heat transfer coefficient (unit, W), and T_a is the temperature of the fluid flow (unit, °C).

The finite element method (FEM) was applied to analysis with MATLAB pde toolbox (Fig. 1). MATLAB Partial Differential Equation (PDE) Toolbox provides functions for solving PDEs with FEM. One of the PDE form that can be solved with the toolbox is described in Eq. 4 [15].

$$m\frac{\partial^2 u}{\partial t^2} + d\frac{\partial u}{\partial t} - \nabla\cdot(c\nabla u) + au = f \tag{4}$$

Where m, d, c, a, and f are user-definable coefficients, and can be defined by function u is the solution function; t is time.

For the studied transient heat transfer process, the boundary conditions are Neumann condition. The generalized Neumann boundary condition form Eq. 5 [15] and can be applied in MATLAB PDE toolbox.

$$\vec{n}\cdot(c\nabla u) + qu = g \tag{5}$$

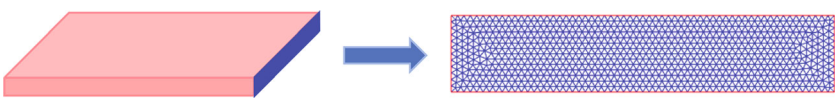

Fig. 1 The product slab with cross-section highlighted (blue area) and the cross-section with mesh for Finite Element Analysis shown

Where $\vec{n}$ is the outward unit normal, c is a user-definable coefficient, and it is of the same value as that in Eq. 4. Both q and g are user-definable functions; u is the solution function.

The governing equation of this process Eq. 1 can be written in the form of Eq. 4, and the convection boundary condition Eq. 3a to 3d can be written in the Neumann boundary condition form in Eq. 5.

The initial temperature for the geometry was set as −18 °C, and different combinations of ambient temperature and convective heat transfer coefficients were tested to study the effects of tempering condition on tempering results. The maximum mesh size was set to 0.005, and the relative tolerance and absolute tolerance were both set to 1×10^{-6}. MATLAB 2018b was run on a computer with 8.00 GB RAM and Intel(R) Core(TM) i5-7200U CPU for this study.

Materials and Methods

Materials

For this simulation, the dimensions for an industrial scale product (6 cm×30 cm×70 cm) were applied to mimic the practical tempering process. The compositions for the products that were analyzed are listed in Table 1 [24–26].

The illustrations in Section "Results and Discussion" were mostly based on pork loin. Pork belly and pork fat were introduced to demonstrate the effects of fat content on time-to-temper.

Methods

Product Freezing Point Prediction

The freezing point of the products was predicted based on the freezing point depression equation. Foods can be treated as ideal solutions, and the relationship between the food composition and the freezing point can be described with the following Eq. 6 [20]:

$$\ln a_w = \frac{M_w \lambda_f}{R_g}\left(\frac{1}{T_f} - \frac{1}{T_0}\right) \tag{6}$$

Table 1 Compositions for the analyzed products

Product	Composition (unit, g/100 g product)			
	Water	Protein	Fat	Ash
Pork loin	72.23	21.43	5.66	1.05
Pork belly	36.74	9.34	53.01	0.49
Pork fat	24.76	9.25	65.7	0.51

Where a_w is the water activity of the food, M_w is the molar mass of the water (18.02 kg·kmol^{-1}), λ_f is the latent heat of fusion of water (333.5 k·kg^{-1}), R_g is the gas constant (8.314 kJ·K^{-1}·kmol^{-1}), T_f is the freezing point of the food of which the unit is K, and T_0 is the freezing point of pure water (273.15 K). There exists the relationship $a_w = n_A$ [2], where n_A is the molar fraction of water in food.

In most food products, there exists bound water; it usually bounds with protein or carbohydrates and does not serve as solvent. This part of water may not freeze even when the temperature is as low as −40 °C. A lot of research has been done on the prediction of bound water in foods.

For this investigation, the equation below Eq. 7 [18] was used:

$$X_b = a\cdot X_{carbonhydrate} + b\cdot X_{protein} (a = 0.3, b = 0.45) \tag{7}$$

and as for the products investigated, pork belly and pork fat are of high fat content, and fat does not have strong capability of binding water; thus, it was not taken into consideration. The bound water mass fraction (X_b) was subtracted from the total water mass fraction (X_w) for the calculation of molar fraction of water (n_A). The following equation (Eq. 8) shows the calculation:

$$n_A = \frac{(X_w - X_b)/M_w}{(X_w - X_b)/M_w + \sum_i X_i/M_i} \tag{8}$$

Where X_i and M_i are the mass fraction and molecular weight for each component except for water.

The predicted freezing points for pork loin, pork belly, and pork fat are −1.1 °C, −1.5 °C, and −2.6 °C, respectively. The predicted freezing points were used to generate the relationship between temperature and unfrozen water mass fraction for each product as shown in Fig. 2. This relationship serves as one of the fundamentals for the further prediction of thermophysical properties of the products as described in 1.

Heat Transfer Simulation

The heat transfer simulation was accomplished with MATLAB PDE toolbox as introduced in Section "MATLAB Partial Differential Equation Toolbox". The thermophysical properties, including density, thermal conductivity, and specific heat, are all functions of temperature, and the unfrozen water mass fraction also changes with temperature.

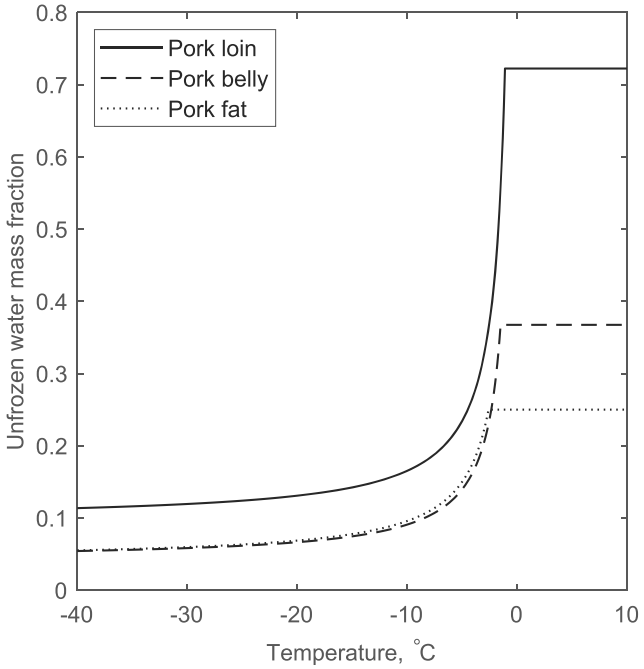

Fig. 2 Unfrozen water mass fraction for studied products

Unfrozen Water Mass Fraction The relationship between temperature and frozen water mass fraction was described with freezing point incorporated (Eq. 9) [20].

$$X_{ice} = \begin{cases} (X_w - X_b)(1 - \frac{T_f}{T}), & T \leq T_f \\ 0, & T > T_f \end{cases} \tag{9}$$

There exists $X_{ice} + X_{uw} = X_w$, where X_w is the total water mass fraction in the food product; thus, the unfrozen water mass fraction (X_{uw}) as a function of temperature is expressed in Eq. 10.

$$X_{uw} = \begin{cases} X_w \cdot \frac{T_f}{T} + X_b \left(1 - \frac{T_f}{T}\right), & T \leq T_f \\ X_w, & T > T_f \end{cases} \tag{10}$$

The unfrozen water mass fraction for each product is shown in Fig. 2.

Density The densities of the products were predicted with Eq. 11 [4].

$$\rho(T) = \left(\sum_i \frac{X_i}{\rho_i(T)} + \frac{X_{ice}(T)}{\rho_{ice}(T)} + \frac{X_{uw}(T)}{\rho_{uw}(T)} \right)^{-1} \tag{11}$$

Where ρ is the density as a function of temperature. X_ice, X_uw, and X_i are the mass fraction of ice, unfrozen water, and other components respectively. The prediction equation for each component developed by [5] in [5] was applied.

Thermal Conductivity Similar to density, thermal conductivity is also a function of temperature. The prediction equation of thermal conductivity is as shown in Eq. 12:

$$k(T) = \rho(T) \left[\frac{X_{ice}(T) k_{ice}(T)}{\rho_{ice}(T)} + \frac{X_{uw}(T) k_{uw}(T)}{\rho_{uw}(T)} + \sum_i \frac{X_i k_i(T)}{\rho_i(T)} \right] \tag{12}$$

For each component, the thermal conductivity prediction equation from [5] was applied.

Specific Heat A smoothened apparent specific heat was applied. The piecewise function of unfrozen water mass fraction Eq. 10 was smoothened with MATLAB function $interp1$ method $pchip$, and the smoothed function is C^1 continuous. The smoothened unfrozen water mass fraction is represented by ξ; thus, the mass fraction of ice is $X_w - \xi$. The enthalpy for water with latent heat of ice fusion taken into consideration is expressed in Eq. 13:

$$H = \int_{T_r}^{T} \left((X_w - \xi) \cdot c_{p_{ice}} + \xi \cdot c_{p_{uw}} \right) \mathrm{d}T + \xi \cdot \left(\lambda_f + \int_{T_0}^{T} \left(c_{p_{uw}} - c_{p_{ice}} \right) \mathrm{d}T \right) \tag{13}$$

Where T_r is the reference temperature. The term $\int_{T_0}^{T} \left(c_{p_{uw}} - c_{p_{ice}} \right) \mathrm{d}T$ does not have a significant influence on the specific heat; thus, it was neglected for calculation simplification. The specific heat of the water-ice mixture was calculated by taking the first-order derivative of enthalpy H as described in Eq. 14:

$$c_{p_{water-ice}}(T) = \frac{\mathrm{d}H}{\mathrm{d}T} \approx (X_w - \xi) \cdot c_{p_{ice}}(T) + \xi \cdot c_{p_{uw}}(T) + \frac{\mathrm{d}\xi}{\mathrm{d}T} \cdot \lambda_f \tag{14}$$

The specific heat for water is predicted by Eq. 15 [20].

$$c_{p_{uw}} = 6.6353 \times 10^5 z^2 - 1.2132 \times 10^4 z + 4231.0$$
$$z = \frac{1}{T + 54.15} \tag{15}$$

as the error between the predicted values and accepted values is within 1% including at 0 °C, where equation failed to maintain a reasonable error [20]. The specific heat for other components was predicted with the classical equations [5].

Thus, the overall specific heat for the product is:

$$c_p(T) = \sum_i X_i c_{p_i}(T) + c_{p_{water-ice}}(T) \quad (16)$$

Targeted Tempering Condition Confirmation

Convective Heat Transfer Coefficient (*h*) The convective heat transfer coefficient is affected by several factors, such as fluid type, fluid velocity, and the geometry of the object. These factors can be connective with convective heat transfer coefficient (h) through a series of dimensionless number, such as Reynolds number (Re), Prandtl number (Pr), and Nusselt number (Nu) [10]. A set of velocities for air flow and water flow were assumed and the h value was calculated. The calculations showed that the convective heat transfer coefficients spread a wide range as the type and velocity of the fluid flow vary.

In this study, the convective heat transfer coefficients studied are 5, 10, 15, 20, 30, 40, 50, 100, 200, 400, 800, 1000, and 2000 $W{\cdot}m^{-2}{\cdot}K^{-1}$.

Ambient Temperature (T_a) The fluid flow temperature is considered ambient temperature in this case. The ambient temperatures −7, −5, −3, −1, 0, 2, and 4 °C were studied. The temperature distributions across the products with and without phase change involved were investigated and compared.

Results and Discussion

Definition of Time-to-Temper

The solution for a heat transfer equation is temperature as a function of time and location. For this study, the temperatures at the surface, midpoint, and center are of significant study interest, and are defined in Fig. 3.

For a convective heat transfer process, the temperature at the surface of the object usually increases the fastest. The time-to-temper is defined as the time required for a frozen product to reach a target temperature at the slowest warming location, and with less than 1 °C temperature difference between the surface and the slowest warming location within the product. For the studied case, the lowest temperature location is the center. An example temperature profile and the time-to-temper defined are as shown in Fig. 4. With the definition, the effects of different factors as target temperature, tempering fluid temperature, convective heat transfer coefficient, product dimensions, and product compositions were studied and discussed.

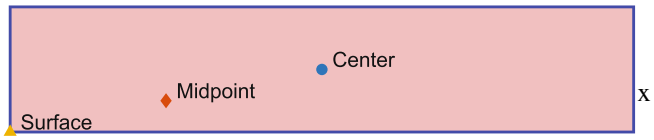

Fig. 3 The surface, midpoint and center studied

For Different Convective Heat Transfer Coefficients (*h*)

The illustration was made based on the pork loin, of which the predicted freezing point is −1.1 °C.

The time-to-temper for T_a under −7, −5, −3, −1, 0, 2, and 4 °C and as a function of h is as shown in Fig. 5. It can be easily concluded that after h reaches 200 $W{\cdot}m^{-2}{\cdot}K^{-1}$, the increase in h value will no longer reduce time-to-temper significantly. In the region where h is between 0 and 200 $W{\cdot}m^{-2}{\cdot}K^{-1}$, the effects that h has on time-to-temper vary more. Similar phenomena have been observed in a pork leg thawing study conducted at 10, 20, and 30 °C [1]. Ambient temperatures in a lower range were investigated in the presented study, and it is shown that no matter the ambient temperature (T_a) is higher than the product's freezing point or lower, the turning point for h-value being an important factor that affects time-to-temper is similar.

In the industry, water and air are the two most frequently used tempering media. Agitation is usually used to increase the convective heat transfer coefficient (h). The time-to-temper vs. h-value relationship found in this study indicates that mild agitation of the tempering media may be beneficial for reducing time-to-temper; however, vigorous agitation will not improve tempering efficiency significantly.

The studied T_a can be divided into three groups, and the effects of h-value on time-to-temper for each group are demonstrated in greater detail at representative temperatures

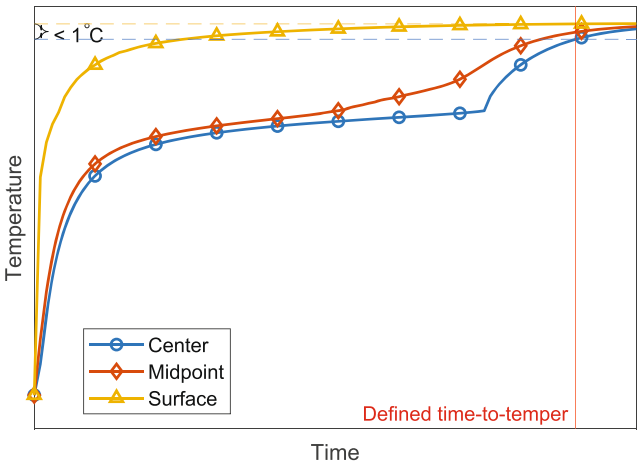

Fig. 4 The definition of time-to-temper based on temperature distribution

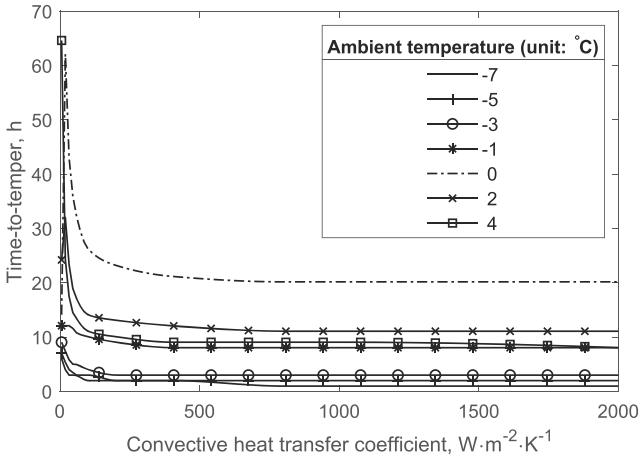

Fig. 5 The effects of convective heat transfer coefficient on time-to-temper for pork loin

−3, 0, and 4 °C in Fig. 6, correspondingly. When T_a is lower than 0 °C, the time-to-temper decreases as h increases. When T_a is in the [0, 4)°C region, the time-to-temper increases before h =20 W·m^{-2}·K^{-1} but decreases afterward. And for T_a = 4°C, the time-to-temper also decreases as h increases, but it starts at a dramatically high value. The differences in the changing trend of time-to-temper with h-value can be explained by the definition of time-to-temper (defined in 1) and the T_a value for each case.

Time-to-temper was defined based on the temperature difference between product surface temperature (T_s) and the slowest warming position temperature (T_{cold}); however, when the h-value is relatively low, the difference between T_s and ambient temperature (T_a) may still be remarkable. Therefore, it is possible that when the tempering is completed by definition, the difference between T_a and T_{cold}, which is defined as T_{ac} ($\Delta T_{ac} = T_a - T_{cold}$), is still greater than 1 °C (Fig. 7).

Under the condition of T_a = 0 °C, when h-value was 20 W·m^{-2}·K^{-1}, ΔT_{ac} was around 4.5 °C, and because the freezing point of the product was −1.1 °C, it can be inferred that the product had not gone through phase change when the tempering was accomplished. Under the same T_a, when h-value was 50 W·m^{-2}·K^{-1}, ΔT_{ac} was less than 1 °C, which indicates that the product had gone through phase change. When product temperature was increasing, the ice content in the product decreased. Ice has higher thermal conductivity (k), lower density (ρ), and lower specific heat (c_p). According to the definition of thermal diffusivity (α), which is a measure of the heat diffusion rate within the product, in Eq. 1, α decreases when temperature increases before reaching the product freezing point, and after the freezing point, α stays nearly constant at the lowest value. T_{cold} when h = 20 W·m^{-2}·K^{-1} was lower than that when h = 50 W·m^{-2}·K^{-1}, and was below freezing point. Therefore, when h = 20 W·m^{-2}·K^{-1}, product surface temperature increased relatively slowly, heat diffused within the product faster, and temperature at different locations increased more uniformly, but when h = 50 W·m^{-2}·K^{-1}, product surface temperature increased faster and passed the freezing point rapidly, thermal diffusivity drastically decreased and led to slow heat diffusion into the product; thus, the temperature across the product increased less uniformly. When h-value was over 50 W·m^{-2}·K^{-1}, T_{cold} reached a similar value to that when h = 50 W·m^{-2}·K^{-1}, but higher convection at the surface provided higher heat flux; thus, the temperature increasing rate across the product was correspondingly higher, which contributed to the decrease in time-to-temper.

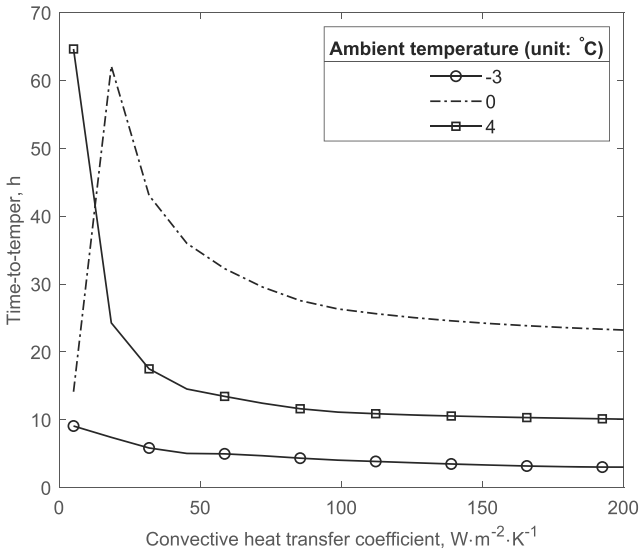

Fig. 6 The effect of convective heat transfer coefficient in the range of 0 –200 W·m^{-2}· K^{-1} on time-to-temper for pork loin

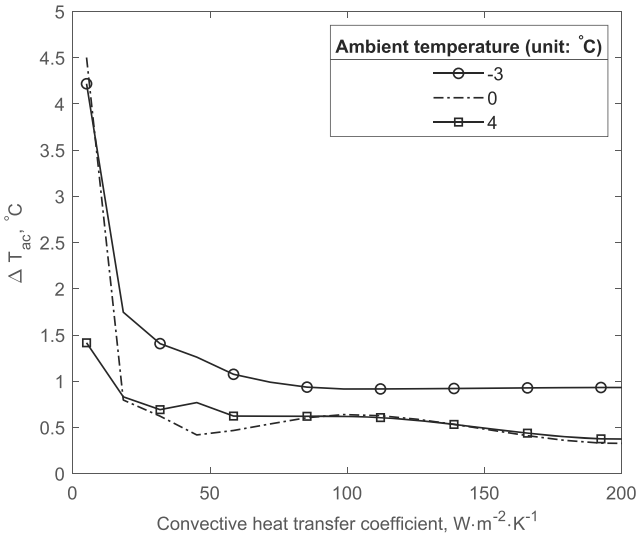

Fig. 7 The difference between lowest temperature location temperature and ambient temperature at time-to-temper when h = 0–200 W·m^{-2}· K^{-1}

For T_a = 4 °C, when h = 5 W·m^{-2}·K^{-1}, ΔT_{ac} = 1.5 °C, when h-value increases, ΔT_{ac} drops below 1 °C. The product went through phase change at h = 5 W·m^{-2}·K^{-1} with the sufficient heat transfer driving force provided by the difference of T_a and initial T_s, resulting in low thermal diffusivity, and leading to the extended time-to-temper. The increase in h-value balanced off the effects by low thermal diffusivity, and the higher the h-value the lower the time-to-temper.

As for the case where T_a = −3 °C, no phase change thoroughly happened across the product during the process. Although the thermal diffusivity was high for h = 10 W·m^{-2}·K^{-1}, but the driving force and convection effect were both low for this situation, contributing to the longer time-to-temper. When the convection increased, the heat transfer efficiency could be improved while thermal diffusivity remained high; therefore, time-to-temper was reduced effectively.

This analysis demonstrated that heat transfer process is controlled by both the product properties and the external conditions from a practical standpoint.

For Different Ambient Temperature (T_a)

The illustration was made based on the pork loin, of which the freezing point is −1.1 °C.

The effects of ambient temperature on time-to-temper under representative convective heat transfer coefficient, 5, 10, 15, 50, and 200 W·m^{-2}·K^{-1}, are as shown in Fig. 8. Ambient temperature ranges from −7 to 4 °C as discussed in the section "For Different Convective Heat Transfer Coefficients (h)".

Along the ambient temperature axis, it can be found that all the curves intersect around T_a = −1 °C.

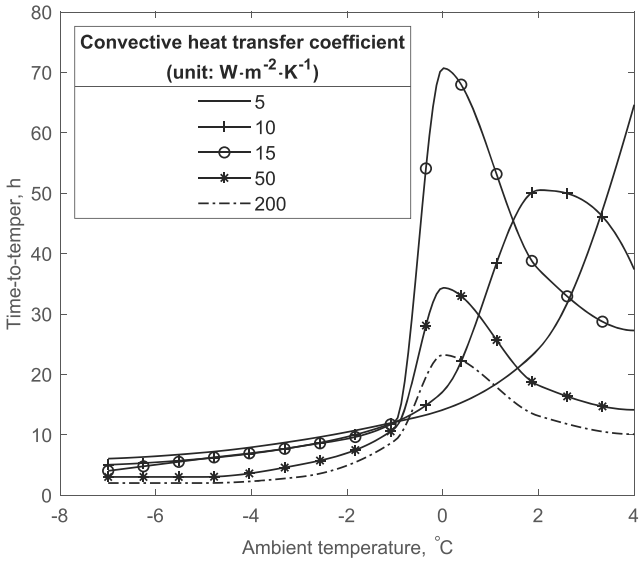

Fig. 8 The effect of ambient temperature on time-to-temper for pork loin

Before T_a reached −1 °C , under each h-value, time-to-temper increased as T_a increased, and for each ambient temperature, time-to-temper showed the trend that the greater the h, the smaller the time-to-temper, which corresponds to what has been discussed in 1. The freezing point of the product is −1.1 °C; therefore, when T_a was below −1 °C, most part of the product had not passed through phase change. The lower the temperature of the product, the higher the ice content of it; therefore, the thermal diffusivity (α) was also higher. The difference between surface temperature (T_s) and slowest warming position temperature (T_{cold}) created when the tempering started could be reduced back to less than 1 °C soon after as α was relatively high, heat diffused across the product rapidly; thus, the temperature at difference locations throughout the product increased at a similarly high rate. Based on this comparison, it could be summarized that when T_a was below the product freezing point, lower T_a allowed the product to be tempered more uniformly. Even for h-value as low as 5 W·m^{-2}·K^{-1}, the high α still allowed the tempering goal to be reached rather fast, resulting in comparatively low time-to-temper. Also because of the synergistic effect of low-h, the increase in time-to-temper with T_a rising was the least significant for h = 5 W·m^{-2}·K^{-1}, as even though α decreased as temperature increases, T_s increased at a lower rate when h is low; therefore, the uniformity of temperature increasing across the product could be maintained to a certain extent under higher T_a.

When T_a was above −1 °C, the effects of T_a on time-to-temper varied. When h = 5 W·m^{-2}·K^{-1}, time-to-temper had the highest value when T_a = 4 °C. For h = 10 W·m^{-2}·K^{-1}, the highest time-to-temper values appear at T_a = −2 °C. When h = 15, 50, 200 W·m^{-2}·K^{-1}, time-to-temper peaked at T_a = 0 °C. The variety among these trends could also be explained by the different T_{cold} when tempering was completed. According to Fig. 8, when h = 5 W·m^{-2}·K^{-1}, T_a = 4 °C, ΔT_{ac} was less than 1.5 °C, but when T_a = 0 °C, ΔT_{ac} was more than 4 °C. When T_a was high, T_s had the tendency to approach T_a first. At T_a = 4 °C, ice in the surface layer quickly melted as T_s passes the freezing point due to the high heat transfer driving force provided by the high T_a, forming a water layer that had lower thermal conductivity than ice, which hindered heat to diffuse further into the product. At the same time, the product showed a tendency to pass through phase change, which indicates that the heat diffused into the product would also be used for overcoming the latent heat of ice fusion, as described in Eq. 13. The closer the temperature approached product freezing point, the higher the amount of heat required for overcoming the latent heat barrier. Most heat absorbed would be distributed to satisfy the latent heat requirement instead of temperature increasing and, consequently, temperature rose at a rather

low rate. Furthermore, the low convection was not able to provide sufficiently high heat flux to accelerate heat diffusion. The peak for the case at h = 10 W·m^{-2}·K^{-1}, T_a = 2 °C could be explained similarly. For T_a = 2 °C, the increase in h-value causes T_s to approach T_a more rapidly; thus for the other part of the product, in order to meet the tempering goal, phase change needed to be overcome to reach the uniformity in temperature distribution. As for T_a = 4 °C when h = 10 W·m^{-2}·K^{-1}, the increase in h-value introduced higher heat flux, contributing to the decrease in time-to-temper. When h increased above 15 W·m^{-2}·K^{-1}, for T_a above freezing point, ΔT_{ac} fell below 1 °C, indicating when the tempering was over, the entire product had gone through phase change, and T_s almost equalled to T_a. A similar reason could explain the peak at T_a = 0. The effect of increasing h-value on reducing time-to-temper discussed in 1 could be observed from this aspect too (Fig. 8).

Based on the comparison between the pre-freezing-point T_a and post-freezing-point T_a, it has been found that using h-value enhancement as a time-to-temper reduction strategy has different effects for different T_a. For the former, increasing h-value usually shortens time-to-temper. For the latter, a greater magnitude of variation and deviation in time-to-temper may be caused by changing h-value due to phase change in this T_a range, and whether time-to-temper can be reduced is determined by the interaction between T_a and h. Generally, T_a below freezing point yields to lower time-to-temper.

For Different Product Compositions

The illustrations were made based on the comparison of time-to-temper for pork loin, pork belly, and pork fat. The compositions for the three products are as shown in Table 1. Pork loin has the lowest fat content, highest protein content, and highest water content, while pork fat has the highest fat content, lowest protein content, and lowest water content. In this comparison, the influence of T_a on time-to-temper was discussed with the h-value at 800 W·m^{-2}·K^{-1}, in which way it can be guaranteed that the difference between T_s and T_a negligible, and the tempered products of all compositions will be of similar temperature. The results are as shown in Fig. 9.

The freezing point for pork loin, pork belly, and pork belly are −1.1, −1.5, and −2.6 °C, respectively, which can be referred to in Fig. 2. From Fig. 9, it was found that the time-to-temper vs. T_a curves for the three compositions are of similar shape. The longest time-to-temper appears when T_a was around 1 °C higher than the freezing point of the product. The magnitude of time-to-temper change due to the change in T_a was the greatest for pork loin and the smallest for pork fat. When T_a was at −7 °C, time-to-temper had the minimal value for pork loin, while that for pork belly and pork fat was similar. When T_a was at 4 °C, pork loin had the greatest time-to-temper and pork fat had the smallest.

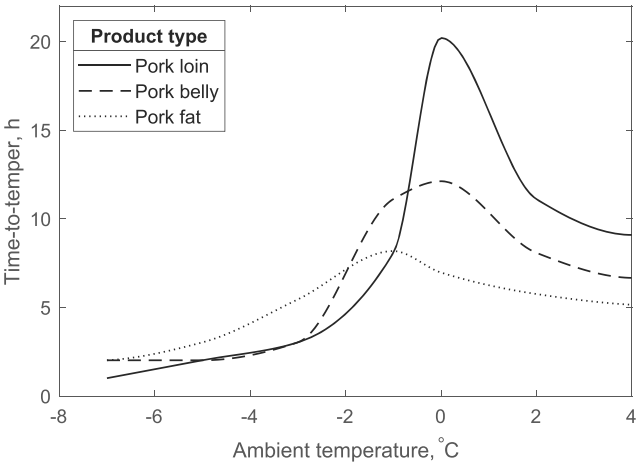

Fig. 9 The effect of ambient temperature on time-to-temper for different pork products when h = 800 W·m^{-2}·K^{-1}

The existence of the peak in time-to-temper could be explained by similar reason as discussed in 1. The difference in the magnitude of time-to-temper among different products was mainly contributed by the difference in water content. For pork loin, which is of higher water content, the latent heat that needed to be overcome when going through phase change was higher, the specific heat of the product when approaching freezing point was correspondingly higher, which resulted in lower thermal diffusivity (α). As for this tempering process, the heat fluxes were the same, thus lower α led to longer time to meet the same target temperature of tempering. When temperature increased, the ice content of the product decreased; therefore, α also decreased. But for product like pork fat with lower water content, the effect on α brought by change in ice content during the temperature increase would not be as significant as that for product with higher water content. Therefore, even when T_a was increasing, for pork fat, α would not decrease too much; thus, the time-to-temper for pork fat would not increase as significantly as that for pork loin.

The difference in the time-to-temper comparison among the three types of products at $T_a = -7$ °C and $T_a = 4$ °C was also due to the difference of water/ice content. Ice is of high thermal conductivity (k), which contributes to α positively, while water is of high specific heat (c_p), which contributes to α negatively. When $T_a = -7$ °C, according to Fig. 2, the unfrozen water mass fractions of pork fat and pork belly around −7 °C were similar; thus, α of pork fat and pork belly was similar, leading to similar time-to-temper. The unfrozen water mass fraction of pork loin, although higher than both pork belly and pork fat, but due to the high total water content, the ice mass fraction was also

higher; thus, α of pork loin was much higher, resulting in shorter time-to-temper than the other two products. When T_a = 4 °C, the unfrozen water mass fraction (water content) of pork loin was the highest, and that of pork fat was the lowest. The high water content led to low α, resulting in the relatively high time-to-temper in pork loin, compared with the other two products.

For Different Dimensions of the Product

This demonstration was made on pork loin, of which the freezing point is −1.1 °C In the practical production, multiple products may freeze to each other during the storage. This situation can be considered as an increase of the product thickness. The time-to-temper for products of thicknesses under the condition when T_a = 0 °C is as shown in Fig. 10. T_a = 0 °C was chosen because for pork loin product, this T_a leads to the greatest time-to-temper overall.

The relationship between time-to-temper and h-value is similar for products of different thicknesses. Time-to-temper peaked at h = 15 W·m^{-2}·K^{-1}, and would not be reduced significantly after h = 50 W·m^{-2}·K^{-1}. This could be explained by the similar reason as discussed in 1. In the h >50 region, when h = 200 W·m^{-2}·K^{-1}, time-to-temper for product of thickness as 12 cm was around 80 h, and that for product of thickness as 6 cm was about 25 h, and the former was nearly 3 times of the latter. When the product thickness is 18 cm, time-to-temper was around 150 h, which was less than twice that of product with 12 cm thickness and around 6 times that of product with 6 cm thickness. When the product thickness increases by n times, time-to-temper tends to increase more than n times. The width of the product is 30 cm. When the thickness is increasing, for the 2-D heat transfer analysis, the shape of the domain was also changing from more rectangular-like to more square-like, contributing to the non-linear changing in time-to-temper.

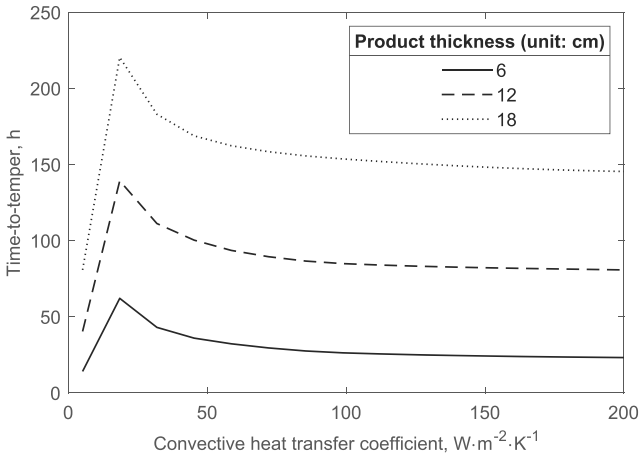

Fig. 10 The effect of convective heat transfer coefficient on time-to-temper for pork loin product of different thicknesses when ambient temperature is 0 °C

Conclusion

In this investigation, "time-to-temper" has been defined as the time when the temperature at the lowest temperature location (T_{cold}) reaches a target temperature while the difference between T_{cold} and product surface temperature (T_s) is within 1 °C. Based on this definition, the conclusions of the research are:

- For the investigated pork loin product, time-to-temper will be significantly reduced when increasing convective heat transfer coefficient from 0 to 200 W·m^{-2}·K^{-1}, further increase will not keep reducing time-to-temper effectively over the studied temperature range from −7 to 4 °C. When having the uniformity in temperature distribution as one of the goals of tempering, low convective heat transfer coefficient can be beneficial. Depending on the ambient temperature, increasing time-to-temper does not necessarily result in reduced time-to-temper.
- For the investigated pork loin product, when ambient temperature is below the freezing point, for the same ambient temperature, the higher the convective heat transfer coefficient is, the lower the time-to-temper; for the same convective heat transfer coefficient, the higher the ambient temperature, the higher the time-to-temper. When ambient temperature is above the freezing point, more variation and deviation are introduced by changing ambient temperature or convective heat transfer coefficient. In general, time-to-temper when ambient temperature is above the freezing point is higher than that when ambient temperature is below freezing point.
- Product composition has significant influence on the time-to-temper. For the investigated pork loin, pork belly, and pork fat products, time-to-temper for the product with lower water content is generally lower than that with higher water content, due to the effect of water phase change on the change of thermophysical properties of product.
- The increase in the product thickness will lead to the increase in time-to-temper. The ratio of time-to-temper increase is higher than that of the thickness increase.

Acknowledgments The authors wish to acknowledge support from the Dale A. Seiberling Endowment in completing portions of the research being presented, and well as the sponsorship from SugarCreek Packing Co.

References

1. Bailey C, James SJ, Kitchell AG, Hudson WR (1974) Air-, water-and vacuum-thawing of frozen pork legs. J Sci Food Agric 25(1):81–97
2. Boonsupthip W, Heldman DR (2007) Prediction of frozen food properties during freezing using product composition. J Food Sci 72(5):254–263
3. Brown T, James SJ (2006) The effect of air temperature, velocity and visual lean (VL) composition on the tempering times of frozen boneless beef blocks. Meat Sci 73(4):545–552
4. Chin SW, Spotar SY (2006) Freezing time prediction for film packaged food. Int J Eng Technol 3(2):182–190
5. Choi Y, Okos MR (1986) Effects of temperature and composition on the thermal properties of foods. Elsevier Applied Science Publishers 1:93–101
6. Choi EJ, Park HW, Chung YB, Park SH, Kim JS, Chun HH (2017) Effect of tempering methods on quality changes of pork loin frozen by cryogenic immersion. Meat Sci 124:69–76
7. Comini G, Cortella G, Saro O (1995) Finite element analysis of coupled conduction and convection in refrigerated transport. Int J Refrig 18(2):123–131
8. Creed PG, James SJ (1981) Predicting thawing time of frozen boneless beef blocks. Int J Refrig 4(6):355–358
9. Delgado AE, Sun DW (2001) Heat and mass transfer models for predicting freezing processes–a review. J Food Eng 47(3): 157–174
10. Çengel YA, Ghajar AJ (2014) External forced convection 5th edn, McGraw-Hill Education, chap 7, pp 424–472
11. Farag KW, Lyng JG, Morgan DJ, Cronin DA (2008) A comparison of conventional and radio frequency tempering of beef meats: effects on product temperature distribution. Meat Sci 80(2): 488–495
12. Hayakawa K-I, Nonino C, Succar J, Comini G, Giudice SD (1983) Two dimensional heat conduction in food undergoing freezing: development of computerized model. J Food Sci 48(6): 1849–1853
13. James SJ, James C (2002) Woodhead Publishing, Thawing and tempering
14. James SJ, James C (2012) Cold store design and maintenance, 2nd edn, CRC Press, chap 9, pp 201–212
15. MATLAB (2019) Partial Differential Equation Toolbox User's guide
16. Mazumder S (2016) The Finite Volume Method (FVM), 1st edn, Academic Press, chap 6, pp 277–338
17. Miao Y, Chen JY, Noguchi A (2007) Studies on the ohmic thawing of frozen surimi. Food Sci Technol Res 13(4):296–300
18. Miles CA, Mayer Z, Morley MJ, HousÆka M (1997) Estimating the initial freezing point of foods from composition data. Int J Food Sci Technol 32(5):389–400
19. Pham QT (2006) Modelling heat and mass transfer in frozen foods: a review. Int J Refrig 29(6):876–888
20. Pham QT (2014) Food Freezing and Thawing Calculations. Springer
21. Piyasena P, Dussault C, Koutchma T, Ramaswamy H, Awuah G (2003) Radio frequency heating of foods: principles, applications and related properties—a review. Crit Rev Food Sci Nutr 43(6):587–606
22. Seyhun N, Ramaswamy HS, Zhu S, Sumnu G, Sahin S (2013) Ohmic tempering of frozen potato puree. Food Bioprocess Technol 6(11):3200–3205
23. Taher BJ, Farid MM (2001) Cyclic microwave thawing of frozen meat: experimental and theoretical investigation. Chem Eng Process Process Intensif 40(4):379–389
24. USDA (2019) Food Composition Databases. https://fdc.nal.usda.gov/fdc-app.html#/food-details/167812/nutrients
25. USDA (2019) Food Composition Databases. https://fdc.nal.usda.gov/fdc-app.html#/food-details/167813/nutrients
26. USDA (2019) Food Composition Databases. https://fdc.nal.usda.gov/fdc-app.html#/food-details/168230/nutrients
27. Wang L, Sun DW (2002) Modelling three-dimensional transient heat transfer of roasted meat during air blast cooling by the finite element method. J Food Eng 51(4):319–328
28. Xiong YL (2017) Lawrie's meat science, 8th edn. The storage and preservation of meat: I thermal technologies, chapter 7, vol 7, pp 205–230